Chinese Journal of Chemical Engineering 56 (2023) 314–324

Contents lists available at ScienceDirect

Chinese Journal of Chemical Engineering

journal homepage: www.elsevier.com/locate/CJChE

Full Length Article

Enhancement of catalytic and anti-carbon deposition performance of SAPO-34/ZSM-5/quartz films in MTA reaction by Si/Al ratio regulation

Jiaxin Wu [1], Chenxiao Wang [1], Xianliang Meng [1,2,*], Haichen Liu [1,2,*], Ruizhi Chu [1,2], Guoguang Wu [1,2], Weisong Li [1,2], Xiaofeng Jiang [1,2], Deguang Yang [1]

[1] School of Chemical Engineering and Technology, China University of Mining & Technology, Xuzhou 221116, China
[2] Key Laboratory of Coal Processing and Efficient Utilization of Ministry of Education, Xuzhou 221116, China

ARTICLE INFO

Article history:
Received 18 April 2022
Received in revised form 18 June 2022
Accepted 19 June 2022
Available online 28 June 2022

Keywords:
Composite zeolite film
Methanol to aromatics
Anti-carbon deposition
Si/Al ratio
Hydrocarbon pool circulation mechanism

ABSTRACT

In order to further improve the catalytic performance of zeolite catalyst for methanol to aromatics (MTA) technology, the double-tier SAPO-34/ZSM-5/quartz composite zeolite films were successfully synthesized *via* hydrothermal crystallization. The Si/Al ratio of SAPO-34 film was used as the only variable to study this material. The composite zeolite material with 0.6Si/Al ratio of SAPO-34 has the largest mesoporous specific surface area and the most suitable acid distribution. The catalytic performance for the MTA process showed that 0.6-SAPO-34/ZSM-5/quartz film has as high as 50.3% benzene-toluene-xylene selectivity and 670 min lifetime. The MTA reaction is carried out through the path we designed to effectively avoid the hydrocarbon pool circulation of ZSM-5 zeolite, so as to improve the aromatics selectivity and inhibit the occurrence of deep side reactions to a great extent. The coke deposition behavior was monitored by thermogravimetric analysis and gas chromatograph/mass spectrometer, it is found that with the increase of Si/Al ratio, the active intermediates changed from low-substituted methylbenzene to high-substituted methylbenzene, which led to the rapid deactivation of the catalyst. This work provides a possibility to employ the synergy effect of composite zeolite film synthesizing anti-carbon deposition catalyst in MTA reaction.

1. Introduction

As an important raw material for organic chemicals and polymer industry, light aromatics have received increasing attention. The methanol to aromatics (MTA) technology not only solves the problem of serious overcapacity of methanol but also provides a new idea for the low-cost synthesis of high-quality aromatics *via* a non-petroleum route [1,2]. The development of catalyst is the key to realizing the practicability of the MTA process.

At present, the main catalysts used in MTA reaction are zeolites. Zeolite catalysts have different specific surface areas and pore structures, which give them unique shape selectivity in different catalytic reactions. Shape selectivity is the key to zeolite catalysis [3,4], and the product distribution strongly depends on structural characteristics. ZSM-5 [5,6], ZSM-11 [7,8], ZSM-22 [9], MCM-22 [10], MCM-36 [10] and H-Beta [11] are the main zeolite catalysts used in MTA reaction. Among them, ZSM-5 zeolite with its ten membered ring pores is the best catalyst for aromatization because its pore size is the same as those of benzene-toluene-xylene (BTX) molecules [12]. If the pore size of zeolite is too small, benzene ring cannot pass through and aromatics cannot diffuse out of the zeolite cage, resulting in carbon deposition [13]. Similarly, SAPO-34 [14] shows excellent selectivity for ethylene and propylene in methanol to olefin (MTO) reaction due to its appropriate pore size. Although studies have shown that ZSM-5 zeolites can rapidly convert methanol to aromatics, pure ZSM-5 zeolites are still prone to carbon deposition and low aromatics selectivity, and cannot meet the needs of industrial production.

In order to solve the problems of using ZSM-5 in MTA reaction, pore channel modification and acidic site improvement have been intensively studied. Among them, the main way to ameliorate the pore structure is to increase the mesoporous volume. For example, Jacobsen prepared single crystal H-ZSM-5 with a mesoporous structure by using carbon black as a hard template [15]. Some scholars [16,17] have used a steam-assistant method to prepare mesoporous ZSM-5. And then, some others [18] have used tetrapropylammonium hydroxide as a post-treatment agent for ZSM-5, the destruction increased the mesoporosity and the strong

* Corresponding authors.
E-mail addresses: meng27@cumt.edu.cn (X. Meng), 4037@cumt.edu.cn (H. Liu).

https://doi.org/10.1016/j.cjche.2022.06.013
1004-9541/

acid density, which inhibited the coke formation and then improved the catalytic stability. Tao *et al.* [19] used homogeneous mesoporous carbon aerogels as a hard template to prepare mesoporous ZSM-5 zeolites, which had mesopores and micropores measuring 11 and 0.51 nm in size, respectively. More researchers have used the metal loading strategy to modify the acidity and acid site distribution of zeolites and adjust their catalytic activity [20–22]. A good linear correlation is observed between the amount of $ZnOH^+$ species and the selectivity to aromatics, suggesting that $ZnOH^+$ species play an important role in enhancing the dehydrogenation of alkanes and the aromatization of alkenes to aromatics [23]. Zhang *et al.* [24] used Cd to modify ZSM-5 by the incipient western invasion method, leading to a reduced number of Brønsted acid sites while generating new Lewis acid sites on the catalysts. The results showed markedly high selectivity of aromatics and low selectivity of light alkanes and C_5–C_9 nonaromatics. Liu *et al.* [25] uzillized embedding method to synthesize ZSM-5/SAPO-34 mesoporous composite zeolites,which had better aromatization activity, and the yield of BTX could reach 30.8%. And Yu *et al.* [26] uzillized mechanical mixing method to prepare SAPO-34/ZSM-5 composite zeolites, which had better reaction stability than ZSM-5 zeolite. In summary, the lifetime of ZSM-5 can be significantly improved by pore modification, the catalytic reactivity can be obviously improved by metal doping and the reaction stability can be improved by composite zeolites. However, few studies have tried to solve the problems by considering the MTA reaction path, which could inhibit the formation of coke deposition from the source. The traditional MTA reaction is composed of multi-step continuous elementary reactions. The reaction process is generally considered to have four important reaction steps: (1) methanol dehydrates to dimethyl ether [27]; (2) Formation of the first C—C bond [28]; (3) The initial C—C species enter the stable reaction period to form a highly active "hydrocarbon pool" intermediate species dominated by methylbenzenes and long-chain olefins [29−32], which generate low-carbon olefins through methylation, alkyl elimination reaction and cracking reaction; (4) Light aromatics are obtained from light olefins through further oligomerization, cyclization, alkylation, hydrogen transfer, and other aromatization processes [33]. Among polymethyl aromatic and long-chain olefins will inevitably continue to undergo deep reactions, resulting in coke deposition covering the active center and blocking the pores.

In this work, based on the confinement effect of zeolite pores, double-tier SAPO-34/ZSM-5/quartz composite zeolite film was designed and developed. According to the high olefin selectivity of SAPO-34 and the high aromatic selectivity of ZSM-5, we divided the MTA reaction path into two parts. In the first layer, methanol is converted into olefins in SAPO-34 crystal layer; The second layer is to aromatize olefins into aromatics in the ZSM-5 crystal layer. And we adjusted the Si/Al ratio of SAPO-34 crystal layer to control the pore channel and acidity of the composite zlityes, then proposed the reaction mechanism for methanol to aromatics with increasing in acidity was proposed. Novel ideas are provided for the development of novel catalysts with improved selectivity and anti-carbon deposition performance in the MTA reaction.

2. Experimental

2.1. Catalyst preparation

ZSM-5/quartz zeolite film was synthesized by hydrothermal synthesis with a gel molar composition of $1SiO_2$: $0.005Al_2O_3$: 0.32TPAOH: $165H_2O$, where sodium metaaluminate (Al_2O_3), tetraethyl orthosilicate (SiO_2) and tetrapropylammonium hydroxide (TPAOH) were employed as the aluminum, silica sources and organic templates, respectively [34]. The precursor was aged at room temperature for 24 h under an appropriate stirring speed. Then, the quartz substrate was parallel put into a hydrothermal crystallization vessel with a Teflon liner, and the synthetic solution was added to the vessel to crystallize at 175 °C for 5 h. After crystallization, the ZSM-5/quartz zeolite film was obtained by washing with deionized water until neutral, drying overnight and removing the organic template in a muffle furnace at 550 °C, with a 0.5 °C·min^{-1} heating rate. The sample after ion exchanging was named HZ-5/K.

SAPO-34/quartz zeolite film was synthesized by hydrothermal synthesis with a gel molar composition of $1Al_2O_3$: $1P_2O_5$: $xSiO_2$ (x = 0.3, 0.6, 0.9, 1.2): 3Mor: $70H_2O$, where aluminum isopropoxide (Al_2O_3), orthophosphoric acid (P_2O_5), tetraethyl orthosilicate (SiO_2) and morpholine (Mor) were employed as the aluminum, phosphorus, silica sources and organic templates, respectively. The crystallization time and temperature are 20 h and 195 °C, respectively. Other experimental operations are the same as those above ZSM-5/quartz film. The sample was named 0.6-S/K.

SAPO-34/ZSM-5/quartz composite zeolite films were synthesized according to the secondary crystallization method. The specific methods are as follows: (1) the precursor of SAPO-34 with different Si/Al ratios was poured into a crystallization kettle for 2 h pre-crystallization at 195 °C; (2) pour out the pre-crystallization solution and stir at room temperature to obtain a certain amount of uniform SAPO-34 microcrystalline suspension; (3) the modified ZSM-5/quartz substrates were put into SAPO-34 microcrystalline suspensions for secondary crystallization for 10 h at 195 °C. After other experimental operations, the composite zeolites with different Si/Al ratios of SAPO-34 were obtained, being x-SZ/K (x = 0.3, 0.6, 0.9, 1.2). The relatively accurate mass ratio of SAPO-34 and ZSM-5 crystal phase content in SAPO-34/ZSM-5 composite catalyst is 1:1.

2.2. Catalyst characterization

The crystal structure of zeolites was measured by X-ray diffraction with a D8 ADVANCE instrument (XRD, Bruker, USA) operating at 40 kV and 45 mA using Cu K_α radiation (λ = 0.15 mm), with a scanning speed and range of 5 (°)·min^{-1} and 5°−50°, respectively. The morphologies of the zeolites were obtained by a GeminiSEM 500 field emission scanning electron microscope (FESEM, SIGMA ZEISS, Germany). The adsorption isotherm was performed by N_2 adsorption measurements on an Autosorb-IQ2 (Quantachrome, USA). Before the measurement, the catalysts were outgassed at 300 °C for 8 h. The total surface area was calculated by the BET method. The pore size distribution was calculated by the DFT method. The t-plot method was applied to obtain the micropore/external surface area and micropore volume. The acidity properties of the catalysts were evaluated by NH_3 temperature-programmed desorption tests performed on a ChemStar^{TM} TPx instrument (NH_3-TPD, Quantachrome, USA). ^{29}Si MAS NMR spectra were obtained on an Advance Bruker 400 M spectrometer (MAS NMR, BRUKER, Germany) operating at a resonance frequency of 104.22 MHz. Chemical shifts were referenced to tetramethylsilane (TMS) for ^{29}Si. Thermal degradation measurements were performed from room temperature to 800 °C with a heating rate of 10 °C·min^{-1} in the air using a STA449F5 thermogravimetric analyzer (TG-DTG, NETZSCH, Germany). The coke composition was analyzed by an Agilent 8890/5977B gas chromatograph/mass spectrometer (GC–MS, Agilent, USA). Before GC-MS measurement, 0.1 g completely deactivated catalyst was treated with 2 ml of HF (40%) followed by extraction with 4 ml methylene chloride to get the organic composition and remove HF.

2.3. Catalytic evaluation

The 0.6 g (the mass of SAPO-34 and ZSM-5 crystal phase content) of sheet catalysts were weighed and filled into a reaction tube

with an inner diameter of 10 mm and a bottom filled with steel wire mesh as support. The temperature of the fixed bed reactor was programmed to 500 °C. The catalyst was activated in the atmosphere of 99.999% high purity N_2 (0.04 MPa) for 2 h. At the end of activation, the temperature of the reactor was reduced to 450 °C and the methanol liquid was injected into the reactor with a WHSV of 2 h^{-1}. The sampling time was 50 min for 20 cycles in total. The composition and distribution of reactants were determined by an external standard method. A KB-PLOT Q plus column (30 m × 0.32 mm) was used to detect C_1–C_5 low-carbon hydrocarbons in the product gas, and the KB-WAX column (60 m × 0.32 mm × 0.50 μm) was used to detect C_6–C_8 aromatics and alcohol ether intermediates in the product gas. The two columns were installed in parallel, and the intake air was sampled at the same time.

3. Results and Discussion

3.1. Catalytic test

The catalytic performance of the catalysts in the MTA reaction was investigated. The selectivity of MTA target products between composite and single zeolites was listed in Table 1, in which two key pieces of information can be obtained: (1) Compared powdered HZ-5 with HZ-5/K film, the proportion of products changed, where selective of BTX was almost unchanged, but selective of alkane and olefins changed. This probably is due to film zeolite being more conducive to the occurrence of alkylation. (2) It can be seen 0.6-S/K has high selective of olefins and no BTX. If we could combine the high olefin selectivity of SAPO-34 with the high aromatics selectivity of ZSM-5 and the aromatization of the film, the aromatics yield would be greatly improved. Excitedly, the products of composite zeolite obviously changed, the BTX selectivity of 0.6-SZ/K film was 15% higher than that of HZ-5/K film. This shows that the ZSM-5 in the composite zeolite can quickly convert olefins to aromatics, while it is obvious that the role of SAPO-34 tier is to convert methanol to olefins. The synergistic effect of high olefin selectivity and high aromatic selectivity of composite zeolite film was successfully realized.

Next, the catalytic performance of the composite zeolites was investigated by changing the Si/Al of SAPO-34. Fig. 1(a) shows the methanol conversions *versus* time-on-stream (TOS) over the catalysts. It can be seen that all catalysts converted the methanol feed completely at the initial stage of the reaction. Among the lifetime of 0.6-SZ/K was significantly higher than that of others. It is speculated that its more developed pore structure may lead to low mass transfer resistance and great carbon deposition resistance. What's more, products of different Si/Al ratios of zeolites are different (Fig. 1(b)). With the increase in Si/Al ratio, the BTX selectivity changed from small to large and then decreased. At SAPO-34 of 0.6Si/Al, the BTX selectivity reached the highest 50.3%. Presumably, it is because the more appropriate acid amount and distribution lead to higher selectivity. At the same time, it is found that the alkane selectivity of the 1.2-SZ/K composite zeolite

Table 1
MTA reaction product distribution of catalysts (TOS = 180 min)

Catalyst	Selectivity/%				
	Alkane C_1–C_5	Olefins C_2–C_5	BTX		
			Benzene	Toluene	Xylene
HZ-5	4.3	60.5	0.4	3.2	31.6
HZ-5/K	9.6	55.3	0.5	3.3	31.3
0.6-S/K	17.3	82.7	–	–	–
0.6-SZ/K	6.9	42.8	0.2	2.2	47.9

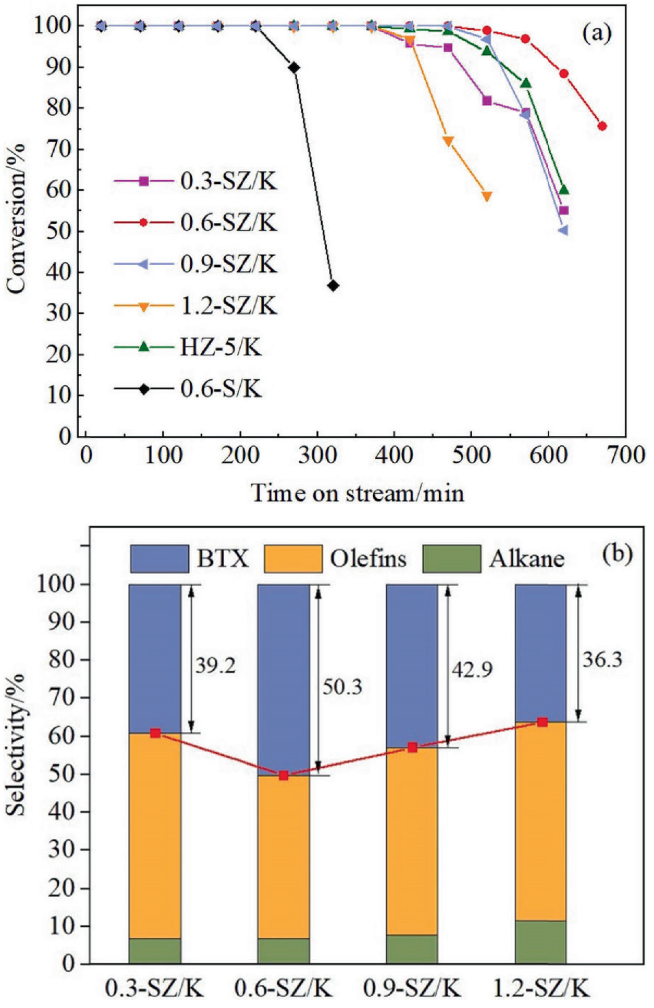

Fig. 1. (a) Methanol conversion of catalysts in MTA reaction with time-on-stream (TOS). (b) Comparison of the selectivity of MTA target products between composite zeolites (TOS = 180 min). Experimental conditions: WHSV = 2 h^{-1}, T = 450 °C, atmospheric pressure.

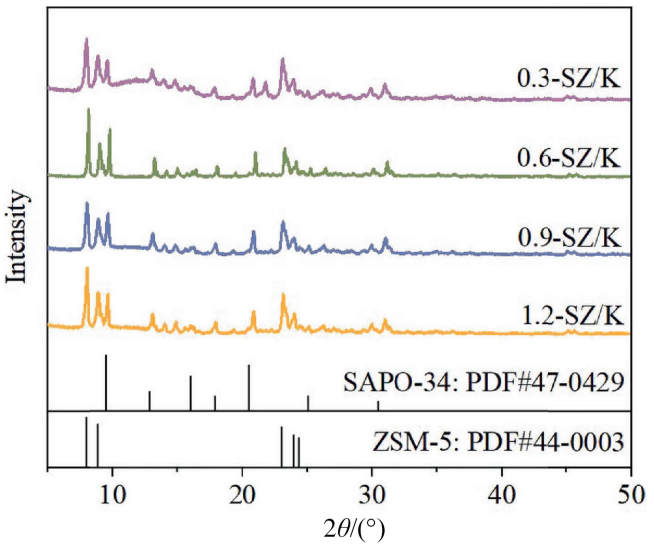

Fig. 2. XRD patterns of *x*-SZ/K composite zeolites.

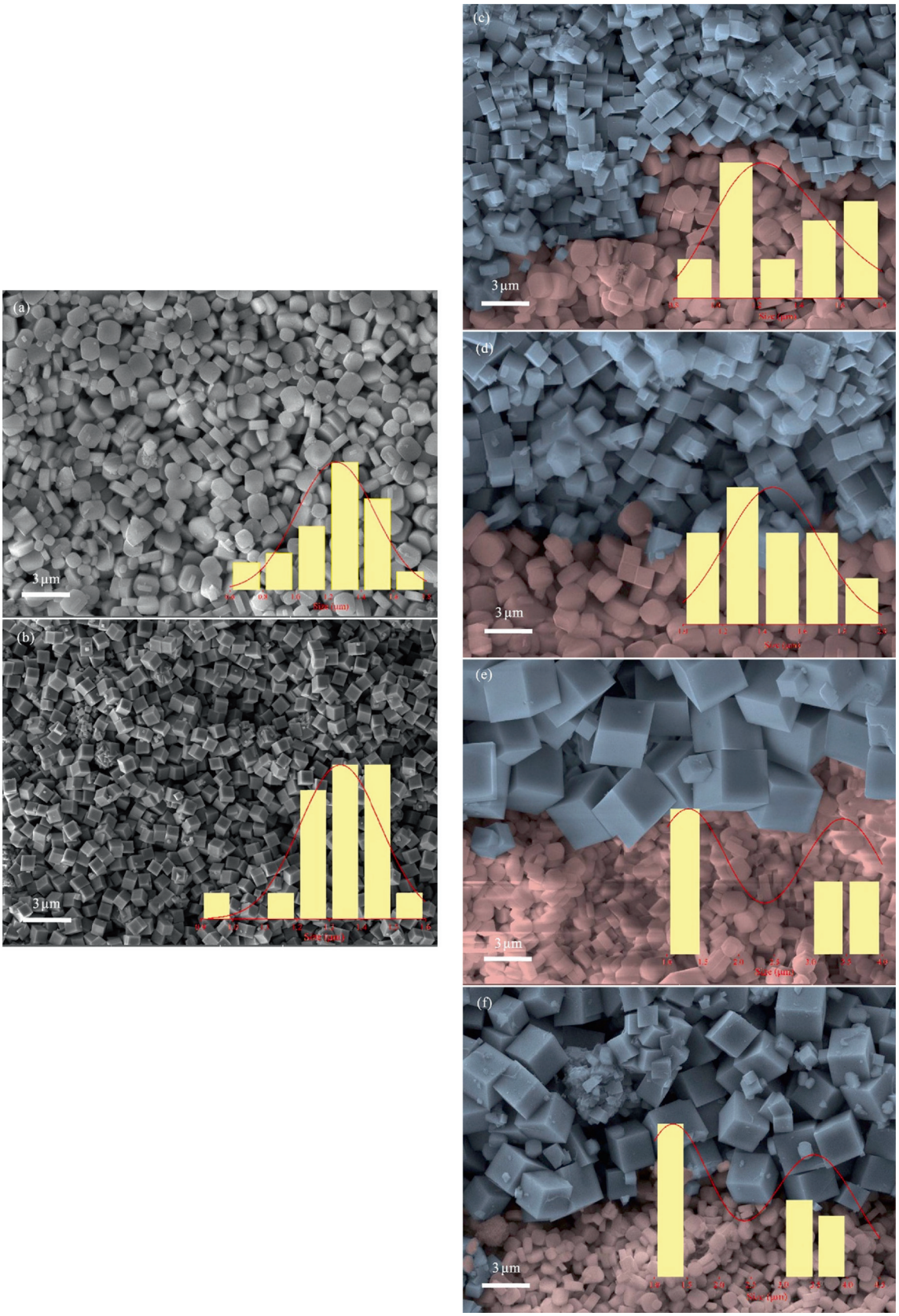

Fig. 3. FESEM images of (a) HZ-5/K zeolite; (b) vertical view of composite zeolite; cross-section views of (c) 0.3-SZ/K zeolite, (d) 0.6-SZ/K zeolite, (e) 0.9-SZ/K zeolite, (f) 1.2-SZ/K zeolite.

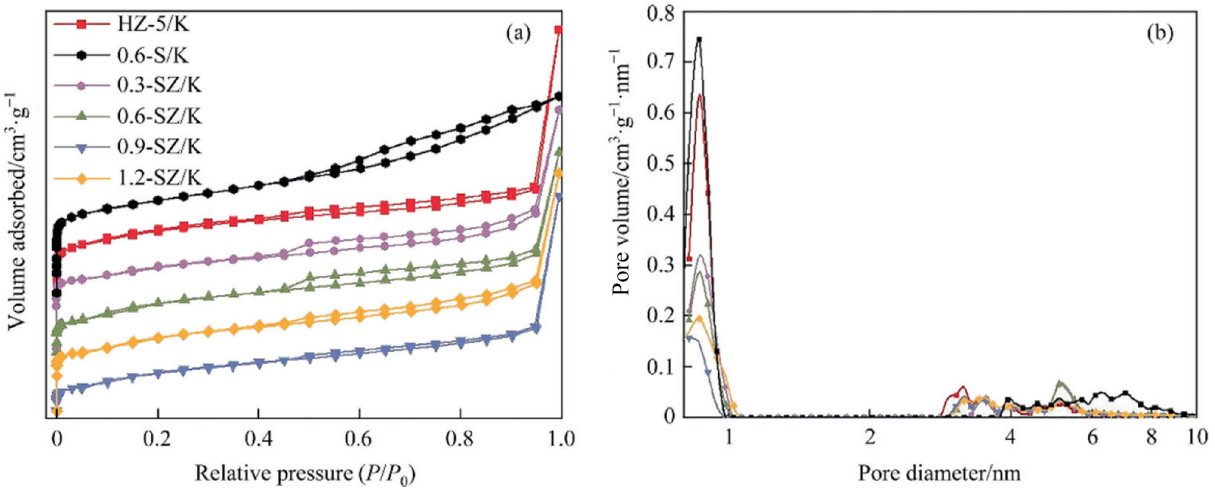

Fig. 4. (a) The N_2 adsorption–desorption curves and (b) BJH pore size distribution of *x*-SZ/K composite zeolites.

Table 2
Structural parameters of *x*-SZ/K composite zeolites.

Catalyst	Surface area/$m^2 \cdot g^{-1}$			Pore volume/$cm^3 \cdot g^{-1}$			Average pore diameter
	S_{BET}	S_{Micro}	S_{Meso}	V_{Toal}	V_{Micro}	V_{Meso}	D_A/nm
HZ-5/K	417.2	288.8	128.4	0.483	0.107	0.376	4.632
0.6-S/K	453.0	426.4	26.6	0.246	0.215	0.031	2.534
0.3-SZ/K	299.3	160.3	139.0	0.368	0.067	0.301	4.916
0.6-SZ/K	283.4	99.5	183.9	0.385	0.036	0.349	5.009
0.9-SZ/K	249.3	87.6	161.7	0.365	0.039	0.326	6.165
1.2-SZ/K	250.4	78.2	172.2	0.362	0.035	0.327	5.783

Note: V_{Micro}, micropore volume determined by *t*-plot; V_{Meso}, mesopore volume determined by $V_{Total} - V_{Micro}$.

was 11.5%, which might be due to alkene alkylation caused by an excessive number of strong acidic sites on the surface.

3.2. Textural properties

The XRD patterns of the *x*-SZ/K composite zeolites are shown in Fig. 2. There are five diffraction peaks at $2\theta = 7.9°$, 8.8°, 23.1°, 23.8°, and 24.4°, which are attributed to the MFI type ZSM-5 zeolite [35], and there are seven diffraction peaks at $2\theta = 9.8°$, 12.9°, 16.0°, 17.9°, 21.3°, 25.1°, and 31.2°, which are attributed to the CHA type SAPO-34 zeolite [36], indicating that SAPO-34/ZSM-5/quartz composite zeolite films were successfully synthesized. It can be seen that the ZSM-5 and SAPO-34 zeolite has high degree of crystallinity, indicating that the structure and crystallinity of HZ-5/K were not obviously damaged when putting it into pre-crystallized SAPO-34 precursor solutions for seed crystal adsorption and secondary growth. Furthermore, characteristic diffraction peaks of ZSM-5 were basically consistent, but there are differences in SAPO-34, which may be the reason for the different catalytic performances. In particular, the diffraction peak at $2\theta = 9.8°$ is obviously higher than that of the others, indicating the exposed (1 0 1) crystal face is the most, which is conducive to catalytic reaction.

The crystal morphology of composite zeolite films was observed by FESEM (Fig. 3). In order to facilitate observation, the crystals were dyed in different color (Fig. 3(c)–(f)). The HZ-5/K zeolite before loading is shown in Fig. 3(a). The ZSM-5 zeolite grains with a 1.0–1.6 μm size were densely arranged on the quartz surface. Fig. 3(b) showed the vertical view of composite zeolite film loaded with SAPO-34 zeolite. The typically cubic SAPO-34 zeolite grains were uniformly and densely loaded on the surface of the ZSM-5/quartz substrate. Fig. 3(c)–(f) show the cross-sections of *x*-SZ/K zeolite films obtained by grinding the composite zeolite films with 2.7 μm sandpaper along the surface at a 45° angle, proving that the zeolite film had a complete composite zeolite film. With the increase in Si/Al ratio, the grain size of SAPO-34 also becomes larger, which leads to a longer mass transfer path, increased carbon deposition, and easy deactivation of the catalyst. When the Si/Al ratio of SAPO-34 is 0.6, the grain sizes of ZSM-5 and SAPO-34 are basically the same, resulting that the film formed is the densest and the catalytic performance is the best. When the Si/Al ratio is 1.2, there are many incompletely grown crystals, which may be the reason for the decline of catalytic performance.

The pore structure parameters of composite zeolites were analyzed by N_2 isothermal adsorption–desorption (Fig. 4). The *x*-SZ/K composite zeolites were classified as type I isotherms. In the low

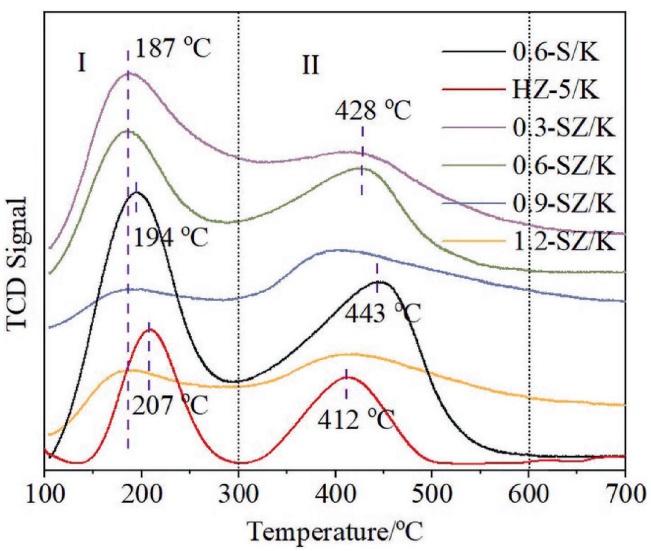

Fig. 5. NH_3-TPD diagrams of *x*-SZ/K zeolite.

Table 3
Acidity data of *x*-SZ/K zeolite

Catalyst	Total acid/mmol·g^{-1}	Weak acid/mmol·g^{-1}	Strong acid/mmol·g^{-1}	Strong acid/weak acid
HZ-5/K	1.264	0.668	0.596	0.89
0.6-S/K	1.617	0.761	0.856	1.12
0.3-SZ/K	1.477	0.972	0.505	0.52
0.6-SZ/K	1.036	0.469	0.567	1.29
0.9-SZ/K	0.867	0.146	0.721	4.94
1.2-SZ/K	0.855	0.196	0.659	3.36

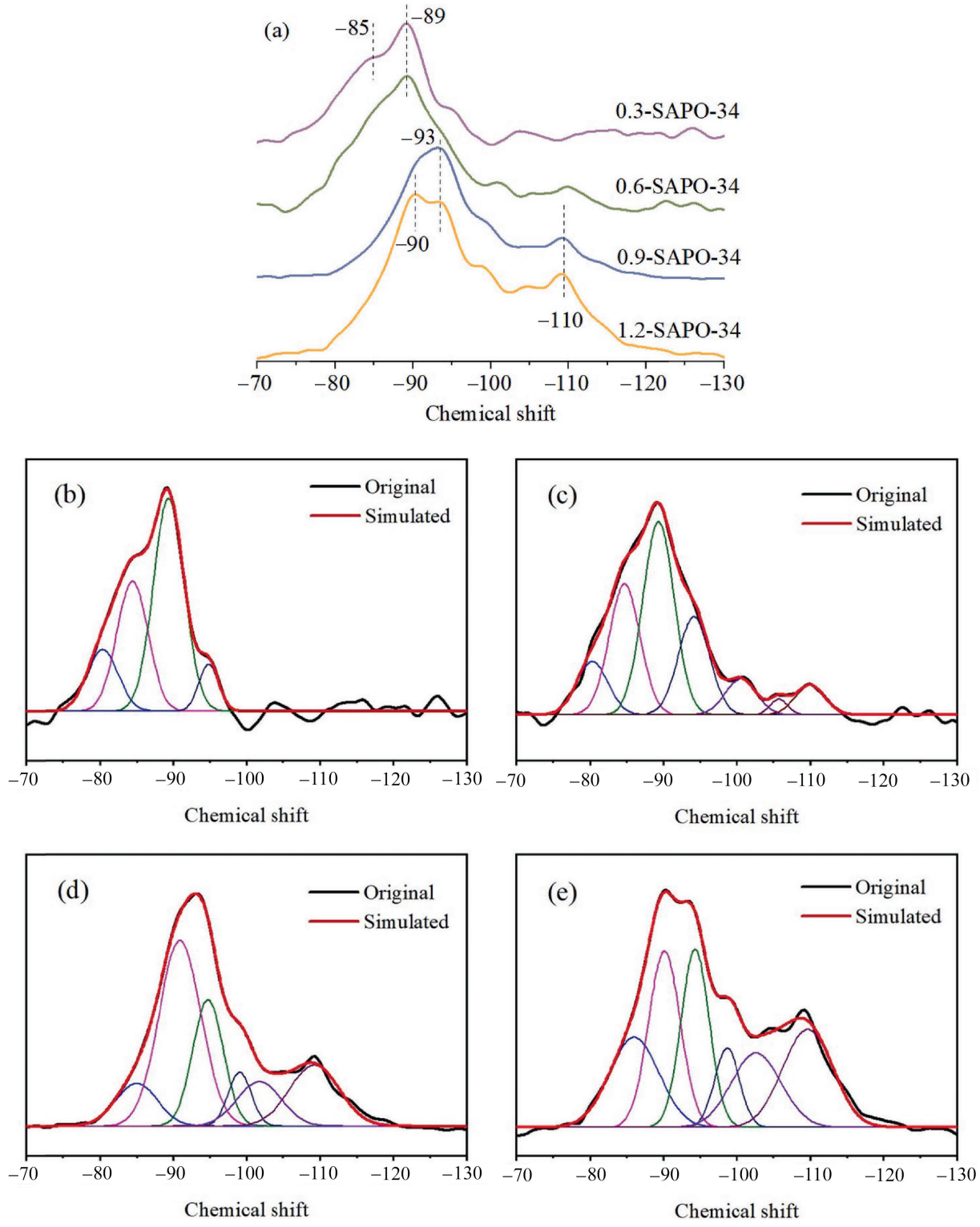

Fig. 6. ^{29}Si MAS NMR spectra of (a) *x*-SAPO-34, (b) 0.3-SAPO-34, (c) 0.6-SAPO-34, (d) 0.9-SAPO-34, (e) 1.2-SAPO-34.

Table 4
Percentage composition of ^{29}Si MAS NMR species in *x*-SAPO-34 framework with different silicon content

Silicon species	Chemical shift	Percentage composition of ^{29}Si species/%			
		0.3-SAPO-34	0.6-SAPO-34	0.9-SAPO-34	1.2-SAPO-34
Defects	−80, −85	34.16	29.59	9.04	17.54
Si4Al	−90	58.98	35.22	39.67	21.67
Si3Al1Si	−95	6.86	19.91	19.52	19.50
Si2Al2Si	−100	0	7.58	6.29	7.74
Si1Al3Si	−105	0	1.57	10.09	14.45
Si4Si	−110	0	6.13	15.39	19.10

pressure region (P/P_0 < 0.04), the isothermal curve rose sharply, indicating that there were a large number of micropores in the zeolites [37]. In the medium and high pressure regions (0.3 < P/P_0 < 1.0), there were different regular shapes belonging to H4 type hysteresis loops, which are mesoporous structures formed by a small number of slit pores in the zeolites crystals. The average pore diameter of *x*-SZ/K zeolites was calculated, where D_A was around 4–6 nm. According to the pore structure parameters of the composite zeolites (Table 2), the specific surface area and pore volume of the composite zeolites changed according to the Si/Al ratio. The micropore specific surface area of 0.3-SZ/K is larger than that of mesoporous, but mesoporous is larger than that of micropore from 0.6 of Si/Al. Surprisingly, 0.6-SZ/K has the largest S_{Meso}, indicating that an increase in mesopore volume can improve the diffusion coefficient of reactants and products, and enhance the overall carbon resistance deposition ability of composite zeolites. With increases in specific surface area and pore volume, the pore structure of the composite zeolite film was greatly improved. This would increase the high mass transfer rate of reactants and intermediates such as methanol, dimethyl ether, and olefins in the pore channels and reduce the diffusion resistance of carbon deposition substances. The S_{BET} decreased with the increase of Si/Al ratio, and decreased significantly from 0.6 of Si/Al. It is speculated that broken crystals blocked the pores, which can be proved from the SEM images.

3.3. Acidic properties

The acid properties of x-SZ/K composite zeolites were characterized by NH_3-TPD (Fig. 5). There are two different desorption peaks in temperature zone I (100–300 °C) and zone II (300–600 °C). The low temperature desorption peak at 187 °C belong to the weak acid site and the desorption peak site of the weak acid was seemly unaffected by the changes in Si/Al ratios. The high temperature desorption peaks around 400 °C belong to the strong acid site and are 20 °C lower than that of pure SAPO-34 zeolite (443 °C). This indicates that the strong acid strength of the composite zeolite decreased, which is beneficial for delaying catalyst deactivation. This can proved by the catalytic performance evaluation experiment. The acidity data of the composite zeolites was derived from the NH_3 desorption curve (Table 3). The total acid content of the zeolite showed a negative correlation with the Si/Al ratio. The suitable acid content and strong/weak acid ratio jointly determine the high lifetime and high selectivity. Surprisingly, the total acid content of 0.3-SZ/K is the highest, but it has poor catalytic performance. In addition, the 1.2-SZ/K of low acid content has less reactive active centers, so the lifetime and selectivity are low. In order to future investigate the deep reasons for the alienation of the acidity properties of zeolites with different silicon content, we compared the MAS NMR spectra of samples (Fig. 6).

Solid state ^{29}Si MAS NMR spectra were presented in Fig. 6. The doping mode of silicon follows SMII and SMIII mechanism [38]. The order of acid strength formed by the different substitution mode of silicon atoms is Si4Si < Si4Al < Si3AlSi < Si2Al2Si < Si1Al3Si [39,40]. The spectral curves with different shapes appear in the range of −80 to −120 (Fig. 6(a)), indicating that different forms of silicon substitution appear in the framework of SAPO-34 with different silicon content, which leads to the alienation of acidity of *x*-SAPO-34. We further fitted and calculated to obtain the silicon species distribution and percentage content (Fig. 6(b)-(e), Table 4). Each zeolite has chemical shifts at −80, −85, −90, −95, −100, −105 and −110, of which −80 and −85 belong to vacancy defects of silicon atoms, and −90 to −110 belong to Si(4−*n*)Al*n*Si species [41,42]. Silicon in 0.3-SAPO-34 basically exists in the form of weakly acidic Si4Al species, which can well explain that the catalytic performance of 0.3-SZ/K with the highest total acid content is not good. 1.2-SAPO-34 contains a large number (19.10%) of Si4Si species, indicating that its silicon atoms mainly exist in the form of large silicon islands that do not provide acidity, resulting in poor catalytic performance (Fig. 1(a)). We also found that the contents

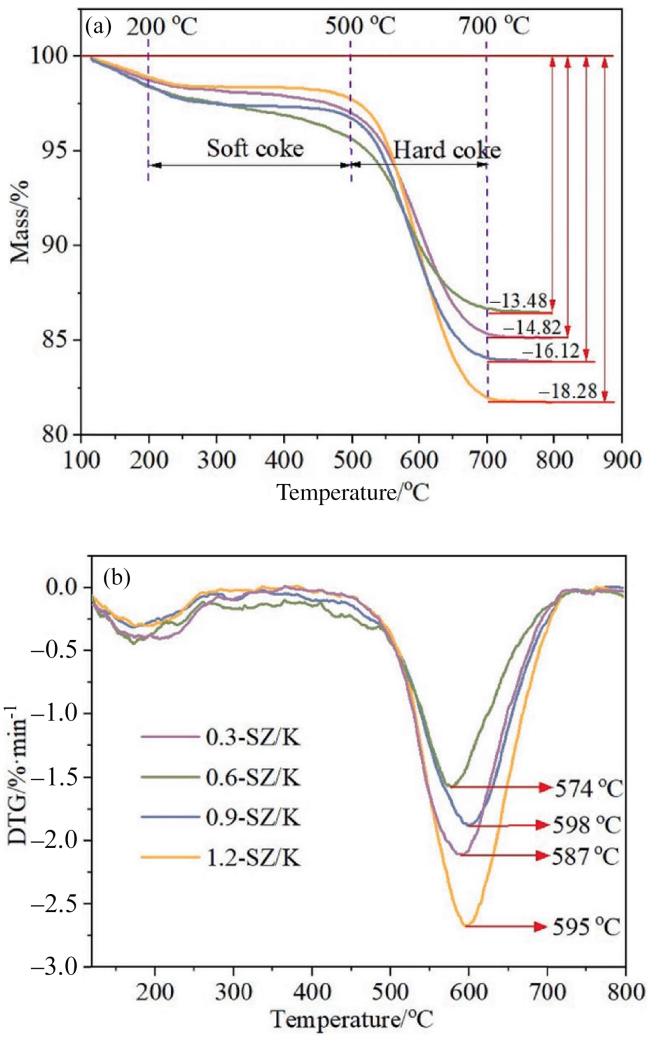

Fig. 7. (a) Thermogravimetric (TG) and, (b) DTG curves of the deactivation *x*-SZ/K.

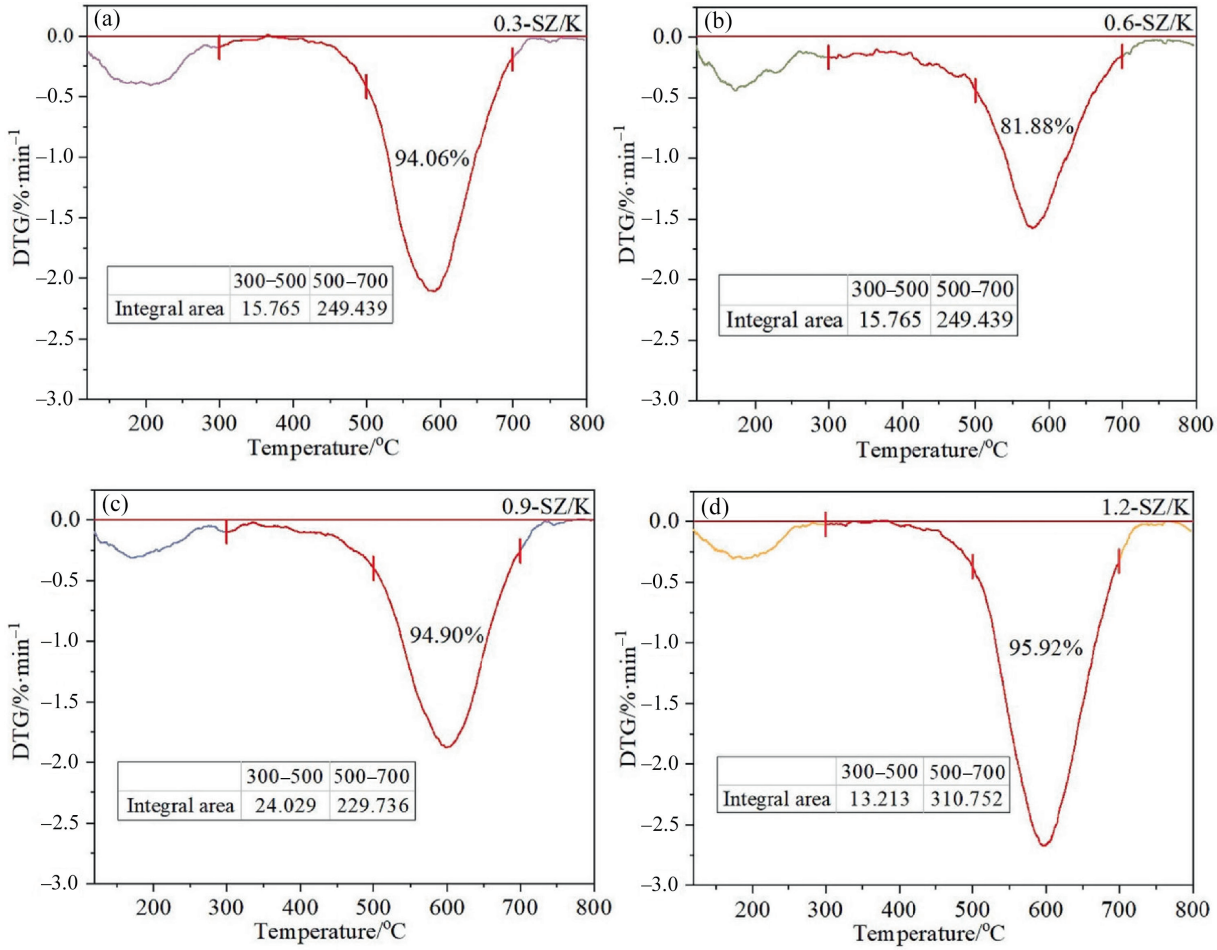

Fig. 8. Piecewise integration of DTG curve of each sample.

of Si4Al, Si3AlSi, and Si2Al2Si in 0.6-SAPO-34, 0.9-SAPO-34, and 1.2-SAPO-34 zeolites are similar, but there are obvious differences in BTX selectivity and lifetime, which is due to the strong acid species Si1Al3Si. A small amount of Si1Al3Si in 0.6-SAPO-34 not only ensures the high selectivity but also maintains its long lifetime.

3.4. Coke deposition analysis

The carbon deposition behavior of *x*-SZ/K composite zeolites was tested by TG analysis (Fig. 7). There are three obvious mass loss temperature ranges as zoned in Fig. 7(a). Among mass loss at 100–300 °C is the evaporation of physically adsorbed water in the zeolite channel, mass loss at 300–500 °C is the decomposition of soft carbon deposition, and mass loss at 500–700 °C is attributed to the decomposition of hard coke deposit. Hard coke deposit belongs to irreversible carbon deposit and can only be burned at high temperature. When the temperature exceeds 700 °C, the mass loss curve tends to be stable, indicating that the decomposition of carbon deposit species is basically completed. Through the mass loss, it can be found that the coke amount of 0.6-SZ/K is the least, indicating that it has good coke deposition resistance. DTG curve (Fig. 7(b)) shows that the maximum mass loss peak corresponding to the lowest temperature of 574 °C belongs to 0.6-SZ/K, indicating that its carbon deposition was decomposed more easily at lower temperature. The amount of soft and hard coke deposition was obtained by piecewise integration of DTG curve (Fig. 8) of each sample. For 0.6-SZ/K catalyst, the amount of soft coke deposition accounts for more of the total coke deposition compared with other catalysts, showing that the tendency of hard carbon formation is lower than that of others and it is easier to remove during coke-burning regeneration. And according to calculating the coking rate (Table 5), we can see 0.6-SZ/K catalyst has the lowest R_{coke}, indicating it can retard the coke formation and thus prolong the catalyst lifetime. Thus, changing the Si/Al ratio has a great impact on the pore structure and acidity of catalysts, which can profound effect on their coke deposition resistance.

Next, we tested the soluble coke deposition of completely deactivated *x*-SZ/K, and the composition of the coke was analyzed by GCMS (Fig. 9). The soluble coke is mainly composed of small molecular aromatics not larger than pyrene derivatives. Coke from different Si/Al ratios of composite zeolites has its characteristics: (1) The monoaromatic hydrocarbons are the main components of coke from 0.3/0.6-SZ/K, however, the concentration of polymethylbenzene in coke from 0.6-SZ/K is also much lower than that from

Table 5
Coking rate of *x*-SZ/K in MTA reaction

Sample	Catalyst mass/g	Reaction time/min	R_{coke}/g^{-1}·min^{-1}
0.3-SZ/K	0.1	370	4.01×10^{-3}
0.6-SZ/K	0.1	470	2.87×10^{-3}
0.9-SZ/K	0.1	470	3.43×10^{-3}
1.2-SZ/K	0.1	370	4.94×10^{-3}

Note: R_{coke} = coke amount/reaction time [43].

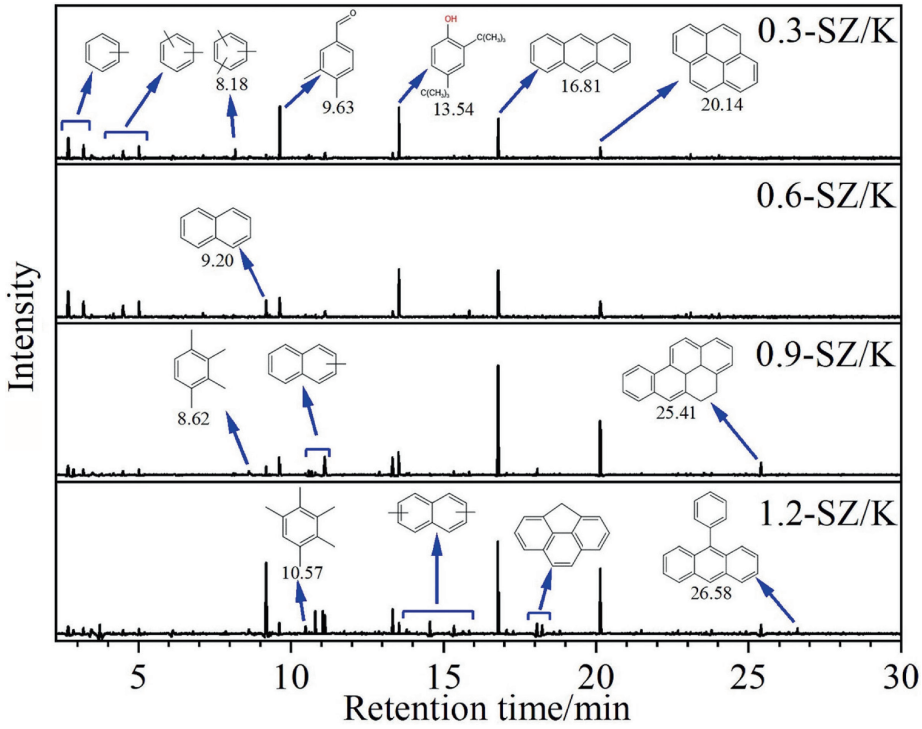

Fig. 9. GC–MS chromatograms of organic coke deposition of deactivated *x*-SZ/K catalyst.

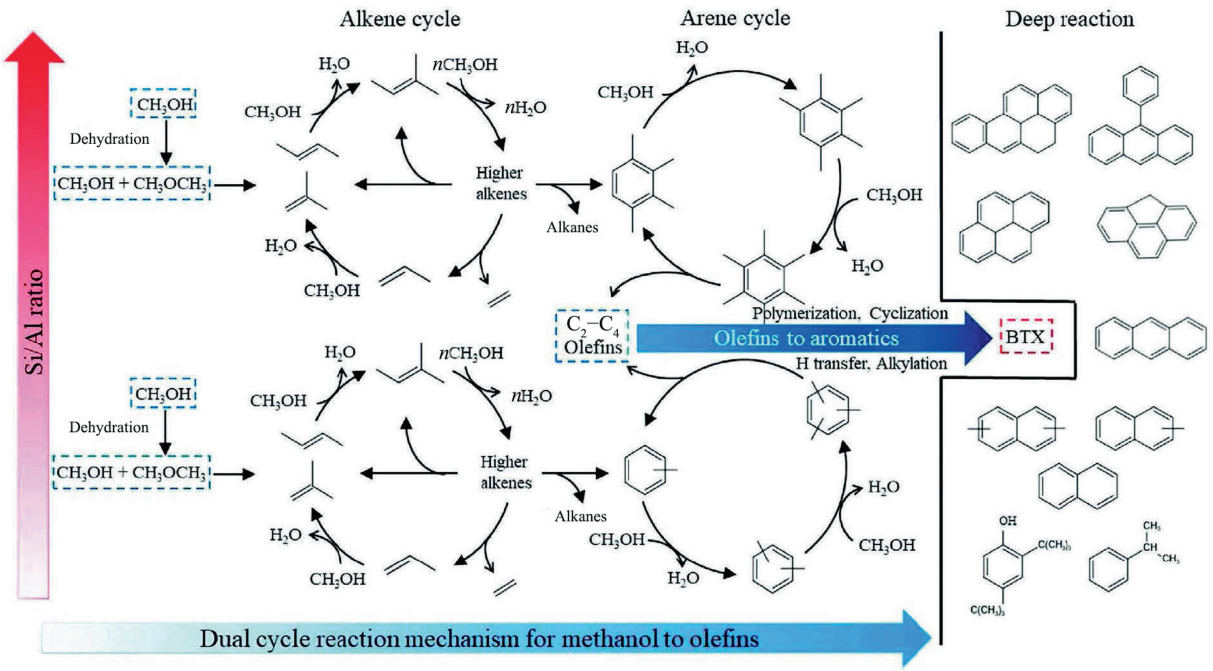

Fig. 10. Reaction mechanism for methanol to aromatics with increasing in Si/Al ratio.

0.3-SZ/K, indicating that the suitable acidity can effectively inhibit the formation of macromolecular coke deposition. (2) For the 1.2-SZ/K catalyst, the largest amount of polycyclic aromatic hydrocarbons (PAHs) appeared, such as naphthalene, anthracene, and pyrene, and also some PAHs derivatives including 4H-cyclopenta (def)phenanthrene were compositions of coke. It is speculated that the important reason for the deactivation of the catalyst caused by strong acidity is the tendency to produce coke of large molecular weight.

3.5. Reaction mechanism analysis

Fig. 10 shows the reaction mechanism for MTA with increasing in Si/Al ratio. First methanol is dehydrated on SAPO-34 film to pro-

duce dimethyl ether, and then the mixture of dimethyl ether and methanol reacts to produce long-chain olefins. A part of long-chain olefins as active intermediates produces a series of low-carbon olefins through multiple methylation and cracking reactions. Most long-chain olefins produce methyl-benzene through polymerization and cyclization. Polymethylbenzene aromatics, as the active center of aromatics-based hydrocarbon pool mechanism, produce light olefins through methylation and alkyl elimination reaction. Then product BTX is produced on ZSM-5 film by olefin aromatization reaction, including polymerization, cyclization, H transfer, and alkylation of light olefins. With the increasing Si/Al ratio of zeolites, the active intermediates in the aromatic-based hydrocarbon pool changed. When the Si/Al ratio is low, the active intermediates are mainly monosubstituted and disubstituted methylbenzene; when the Si/Al ratio is high, the active intermediates are mainly penta substituted and hexa substituted methylbenzene. Also, we found that the higher the Si/Al ratio, the more the soluble coke products developed towards polycyclic aromatic hydrocarbons.

4. Conclusions

In this research, a series of double-tier SAPO-34-ZSM-5/quartz composite zeolite films with different Si/Al ratios were successfully designed, synthesized, and applied to the MTA reaction. The composite zeolite films possess excellent structural characteristics and catalytic performance, which results in high BTX selectivity and a significantly prolonged lifetime. In particular, the 0.6-SZ/K composite zeolite film reaches 50.3% BTX selectivity and has 670 minutes lifetime. This is due to (1) the combination of the high olefin selectivity of the SAPO-34 film and the high aromatics selectivity of the ZSM-5 film, (2) the increased mesopore volume of composite zeolites, which can greatly improve the diffusion coefficient of the reactants and products, shorten the residence time of intermediate products in the zeolites; and (3) suitable distribution of strong and weak acid species. Among, a small amount of Si2Al2Si and Si1Al3Si can promote the conversion of methanol, but it will cause the rapid deactivation once excessive. Subsequently, the coke deposition of deactivation zeolites was investigated by TG and GC–MS, the results demonstrated that 0.6-SZ/K catalyst has the lowest R_{coke} and has lowest PAHs, indicating that it can retard the coke formation and thus prolong the catalyst lifetime. And the species of coke deposition changed greatly with Si/Al ratio. Obviously, with the increase in Si/Al ratio, the coke deposition develops towards polycyclic aromatic hydrocarbons. Mostly important, two reasonable reaction paths with Si/Al ratio increase for MTA reaction were proposed. Therefore, based on the excellent catalytic performance of CHA-MFI composite zeolite film, it is expected to become a promising catalyst material in the field of MTA catalysis.

Data Availability

Data will be made available on request.

Declaration of Competing Interest

The authors declare that they have no known competing financial interests or personal relationships that could have appeared to influence the work reported in this paper.

Acknowledgements

This work is supported by the National Natural Science Foundation of China (51974312, 51974308), and the National Key Research & Development Program of China (2019YFE0100100).

References

[1] T. Li, T. Shoinkhorova, J. Gascon, J. Ruiz-Martínez, Aromatics production *via* methanol-mediated transformation routes, *ACS Catal.* 11 (13) (2021) 7780–7819.
[2] S.S. Ali, H.A. Zaidi, Experimental and kinetic modeling studies of methanol transformation to hydrocarbons using zeolite-based catalysts: A review, *Energy Fuels* 34 (11) (2020) 13225–13246.
[3] X.D. Zhang, K. Yue, R.Z. Rao, J.F. Chen, Q. Liu, Y. Yang, F.K. Bi, Y.X. Wang, J.C. Xu, N. Liu, Synthesis of acidic MIL-125 from plastic waste: Significant contribution of N orbital for efficient photocatalytic degradation of chlorobenzene and toluene, *Appl. Catal. B Environ.* 310 (2022) 121300.
[4] N.P. Lin, Y.S. Gong, R.T. Wang, Y. Wang, X.D. Zhang, Critical review of perovskite-based materials in advanced oxidation system for wastewater treatment: Design, applications and mechanisms, *J. Hazard. Mater.* 424 (2022) 127637.
[5] A. Asghari, M.K. Khorrami, S.H. Kazemi, Hierarchical H-ZSM5 zeolites based on natural kaolinite as a high-performance catalyst for methanol to aromatic hydrocarbons conversion, *Sci. Rep.* 9 (2019) 17526.
[6] R.Z. Chu, D.G. Yang, X.L. Meng, S. Yu, Y.Z. Wan, J.X. Wu, J. Wang, Effect of surface structure and adsorption activity on implanting of *b*-oriented ZSM-5 zeolite film on modified α-quartz substrate, *Front. Chem.* 7 (2019) 636.
[7] M. Juybar, M. Kanmohammadi Khorrami, A. Bagheri Garmarudi, Conversion of methanol to aromatics over ZSM-5/11 intergrowth zeolites and bimetallic Zn-Cu-ZSM-5/11 and Ga-Ag-ZSM-5/11 catalysts prepared with direct synthesis method, *J. Chem. Sci.* 131 (10) (2019) 1–14.
[8] K. Shen, N. Wang, X.D. Chen, Z.H. Chen, Y.W. Li, J.Y. Chen, W.Z. Qian, F. Wei, Seed-induced and additive-free synthesis of oriented nanorod-assembled meso/macroporous zeolites: Toward efficient and cost-effective catalysts for the MTA reaction, *Catal. Sci. Technol.* 7 (21) (2017) 5143–5153.
[9] E. Catizzone, Z. Cirelli, A. Aloise, P. Lanzafame, M. Migliori, G. Giordano, Methanol conversion over ZSM-12, ZSM-22 and EU-1 zeolites: From DME to hydrocarbons production, *Catal. Today* 304 (2018) 39–50.
[10] S. Laforge, P. Ayrault, D. Martin, M. Guisnet, Acidic and catalytic properties of MCM-22 and MCM-36 zeolites synthesized from the same precursors, *Appl. Catal. A Gen.* 279 (1–2) (2005) 79–88.
[11] M. Bjørgen, F. Joensen, K.P. Lillerud, U. Olsbye, S. Svelle, The mechanisms of ethene and propene formation from methanol over high silica H-ZSM-5 and H-beta, *Catal. Today* 142 (1–2) (2009) 90–97.
[12] J.X. Wu, X.L. Meng, R.Z. Chu, S. Yu, Y.Z. Wan, C.C. Song, G.F. Zhang, T. Zhao, Molecular dynamics simulation of the implantation of *b*-oriented ZSM-5 film modified α-quartz substrate surface with different modifiers, *Front. Chem.* 7 (2019) 746.
[13] N. Li, C. Meng, D.H. Liu, Deactivation kinetics with activity coefficient of the methanol to aromatics process over modified ZSM-5, *Fuel* 233 (2018) 283–290.
[14] J. Han, G.J. Yang, H. Ding, X.X. Chen, Revealing inherent factors of SAPO-34 zeolites etching towards the fabrication of hierarchical structure, *Microporous Mesoporous Mater.* 319 (2021) 111067.
[15] C.H. Christensen, K. Johannsen, I. Schmidt, C.H. Christensen, Catalytic benzene alkylation over mesoporous zeolite single crystals: Improving activity and selectivity with a new family of porous materials, *J. Am. Chem. Soc.* 125 (44) (2003) 13370–13371.
[16] Z.H. Wei, L.F. Chen, Q.S. Cao, Z.H. Wen, Z. Zhou, Y.R. Xu, X.D. Zhu, Steamed Zn/ZSM-5 catalysts for improved methanol aromatization with high stability, *Fuel Process. Technol.* 162 (2017) 66–77.
[17] J.W. Wang, X.F. Gao, G.L. Chen, C.M. Ding, Forming pure shaped ZSM-5 zeolite bodies by a steam-assisted method and their application in methanol to aromatic reactions, *RSC Adv.* 9 (49) (2019) 28451–28459.
[18] F. Zhou, Y. Gao, H.X. Ma, G. Wu, C.T. Liu, Catalytic aromatization of methanol over post-treated ZSM-5 zeolites in the terms of pore structure and acid sites properties, *Mol. Catal.* 438 (2017) 37–46.
[19] Y.S. Tao, H. Kanoh, K. Kaneko, ZSM-5 monolith of uniform mesoporous channels, *J. Am. Chem. Soc.* 125 (20) (2003) 6044–6045.
[20] K. Wang, M. Dong, X.J. Niu, J.F. Li, Z.F. Qin, W.B. Fan, J.G. Wang, Highly active and stable Zn/ZSM-5 zeolite catalyst for the conversion of methanol to aromatics: Effect of support morphology, *Catal. Sci. Technol.* 8 (21) (2018) 5646–5656.
[21] D.H. Pan, X.H. Song, X.H. Yang, L.J. Gao, R.P. Wei, J. Zhang, G.M. Xiao, Efficient and selective conversion of methanol to Para-xylene over stable H[Zn, Al]ZSM-5/SiO_2 composite catalyst, *Appl. Catal. A Gen.* 557 (2018) 15–24.
[22] J.X. Wu, X.L. Meng, R.Z. Chu, D.G. Yang, X. Li, S. Yu, J. Wang, Structural effects and catalytic performance of Pd catalysts with micro-mesoporous structure on coal tar hydrodesulfurization, *Microporous Mesoporous Mater.* 316 (2021) 110977.
[23] X.J. Niu, J. Gao, K. Wang, Q. Miao, M. Dong, G.F. Wang, W.B. Fan, Z.F. Qin, J.G. Wang, Influence of crystal size on the catalytic performance of H-ZSM-5 and Zn/H-ZSM-5 in the conversion of methanol to aromatics, *Fuel Process. Technol.* 157 (2017) 99–107.
[24] Y.K. Zhang, Y.X. Qu, D.L. Wang, X.C. Zeng, J.D. Wang, Cadmium modified HZSM-5: A highly efficient catalyst for selective transformation of methanol to aromatics, *Ind. Eng. Chem. Res.* 56 (44) (2017) 12508–12519.
[25] Z.Y. Liu, L. Zhang, M. Wei, K. Wang, H.Y. Wang, Study on preparation of hierarchical porous ZSM-5/SAPO-34 composite molecular sieve and its catalytic performance for methanol aromatization, *Appl. Chem. Ind.* 43 (11) (2014) 1977–1980. (in Chinese)

[26] Y. Yu, L. Zhang, M. Wei, H.Y. Wang, Preparation of SAPO-34/ZSM-5 composite zeolite and its performance in methanol aromatization reaction, *Appl. Chem. Ind.* 44 (3) (2015), 434–437, 441. (in Chinese)
[27] W. Wang, M. Hunger, Reactivity of surface alkoxy species on acidic zeolite catalysts, *Acc. Chem. Res.* 41 (8) (2008) 895–904.
[28] J.F. Haw, W.G. Song, D.M. Marcus, J.B. Nicholas, The mechanism of methanol to hydrocarbon catalysis, *Acc. Chem. Res.* 36 (5) (2003) 317–326.
[29] I.M. Dahl, S. Kolboe, On the reaction mechanism for propene formation in the MTO reaction over SAPO-34, *Catal. Lett.* 20 (3–4) (1993) 329–336.
[30] M. Bjørgen, U. Olsbye, D. Petersen, S. Kolboe, The methanol-to-hydrocarbons reaction: insight into the reaction mechanism from [^{12}C]benzene and [^{13}C] methanol coreactions over zeolite H-beta, *J. Catal.* 221 (1) (2004) 1–10.
[31] W.G. Song, J.F. Haw, J.B. Nicholas, C.S. Heneghan, Methylbenzenes are the organic reaction centers for methanol-to-olefin catalysis on HSAPO-34, *J. Am. Chem. Soc.* 122 (43) (2000) 10726–10727.
[32] M. Bjørgen, S. Svelle, F. Joensen, J. Nerlov, S. Kolboe, F. Bonino, L. Palumbo, S. Bordiga, U. Olsbye, Conversion of methanol to hydrocarbons over zeolite H-ZSM-5: On the origin of the olefinic species, *J. Catal.* 249 (2) (2007) 195–207.
[33] G. Caeiro, R.H. Carvalho, X. Wang, M.A.N.D.A. Lemos, F. Lemos, M. Guisnet, F.R. Ribeiro, Activation of C2–C4 alkanes over acid and bifunctional zeolite catalysts, *J. Mol. Catal. A Chem.* 255 (1–2) (2006) 131–158.
[34] C.X. Wang, J.X. Wu, D.G. Yang, W. Li, X. Li, G.G. Wu, R.Z. Chu, X.L. Meng, Effect of surface modification on SAPO-34 loading on ZSM-5 film for MTA reaction, *Microporous Mesoporous Mater.* 332 (2022) 111663.
[35] X. Li, F. Rezaei, D.K. Ludlow, A.A. Rownaghi, Synthesis of SAPO-34@ZSM-5 and SAPO-34@Silicalite-1 core-shell zeolite composites for ethanol dehydration, *Ind. Eng. Chem. Res.* 57 (5) (2018) 1446–1453.
[36] B. Arstad, A. Lind, J.H. Cavka, K. Thorshaug, D. Akporiaye, D. Wragg, H. Fjellvåg, A. Grønvold, T. Fuglerud, Structural changes in SAPO-34 due to hydrothermal treatment. A NMR, XRD, and DRIFTS study, *Microporous Mesoporous Mater.* 225 (2016) 421–431.
[37] X.D. Zhang, S. Xiang, Q.X. Du, F.K. Bi, K.L. Xie, L. Wang, Effect of calcination temperature on the structure and performance of rod-like $MnCeO_x$ derived from MOFs catalysts, *Mol. Catal.* 522 (2022) 112226.
[38] M. Ghavipour, A.S. Mehr, Y. Wang, R.M. Behbahani, S. Hajimirzaee, K. Bahrami, Investigating the mixing sequence and the Si content in SAPO-34 synthesis for selective conversion of methanol to light olefins using morpholine &/TEAOH templates, *RSC Adv.* 6 (21) (2016) 17583–17594.
[39] D. Barthomeuf, Topological model for the compared acidity of SAPOs and SiAl zeolites, *Zeolites* 14 (6) (1994) 394–401.
[40] J. Tan, Z.M. Liu, X.H. Bao, X.C. Liu, X.W. Han, C.Q. He, R.S. Zhai, Crystallization and Si incorporation mechanisms of SAPO-34, *Microporous Mesoporous Mater.* 53 (1–3) (2002) 97–108.
[41] W.L. Shen, X. Li, Y.X. Wei, P. Tian, F. Deng, X.W. Han, X.H. Bao, A study of the acidity of SAPO-34 by solid-state NMR spectroscopy, *Microporous Mesoporous Mater.* 158 (2012) 19–25.
[42] M. Li, C.F. Zeng, L.X. Zhang, Hydrothermal synthesis of SAPO-5 with novel morphologies from hydrogels containing acetic acid and high concentration of triethylamine under neutral or alkaline conditions, *CrystEngComm* 14 (10) (2012) 3787.
[43] W.L. Jin, B.J. Wang, P.F. Tuo, C. Li, L. Li, H.J. Zhao, X.H. Gao, B.J. Shen, Selective desilication, mesopores formation, and MTO reaction enhancement *via* citric acid treatment of zeolite SAPO-34, *Ind. Eng. Chem. Res.* 57 (12) (2018) 4231–4236.